


Compton scattering mediated by quantum entanglement

Peter Caradonna ^{*}*School of Physics, Engineering and Technology, University of York, YO10 5DD York, United Kingdom*

(Received 12 February 2025; accepted 28 April 2025; published 8 May 2025)

In this paper, the 16 Stokes parameters of a two-photon system are organized into a 4×4 Stokes matrix. This formalism is then applied to analyze the polarization properties of annihilation photons produced by electron-positron annihilation, with a particular focus on their evolution during Compton scattering interactions. The study demonstrates that when one of the subsystems undergoes Compton scattering, quantum entanglement preserves the polarization symmetry between the scattered and noninteraction photons, while in the absence of entanglement, this symmetry is lost. Moreover, the method simplifies the calculation of the joint differential cross section for multiple scattering scenarios and provides a means to characterize the polarization properties of the individual subsystems. These findings highlight the impact of quantum correlations on scattering behavior, and they offer a framework for further investigation into the polarization dynamics of entangled photon pairs.

DOI: [10.1103/PhysRevA.111.053708](https://doi.org/10.1103/PhysRevA.111.053708)

I. INTRODUCTION

Annihilation photons, particularly the pair of 511 keV gamma rays produced during electron-positron annihilation, play a critical role in a wide range of scientific and practical applications. Notably, these photons are generated in a pure, maximally entangled state, meaning that the linear and angular momentum correlations are correlated in a definite way such that when the linear or angular momentum is measured in one photon, the corresponding property of its partner is instantly determined, regardless of the distance between them. This condition can be formally described quantum mechanically using what is known as a Bell state.

In astrophysics, space-based Compton telescope instruments have been instrumental in detecting and studying annihilation photons [1,2]. Notably, the COMPTEL instrument aboard the Compton Gamma-Ray Observatory (CGRO) has provided critical observations of the 511 keV gamma-ray line, particularly from the Galactic Center [3]. These instruments utilize Compton scattering techniques to localize and analyze high-energy gamma rays, thereby offering valuable insights into the processes governing positron annihilation in various astrophysical environments.

In materials science, the detection of annihilation photons in positron annihilation spectroscopy (PAS) is used to probe the microstructure of materials, providing insights into defects, vacancies, and other structural characteristics at the atomic scale [4]. Furthermore, in fundamental physics research, annihilation photons serve as a sensitive probe for testing the predictions of quantum electrodynamics (QED) and the Standard Model, as well as for exploring potential new physics beyond current theoretical frameworks [5,6].

In recent years, there has been a growing global interest in utilizing quantum entanglement to enhance imaging in

positron emission tomography (PET) through the integration of Compton camera technology [7–10]. Research efforts have proposed generalized theoretical frameworks [11–14] to predict the kinematics of annihilation photons while accounting for the impact of entanglement on Compton scattering distributions. Additionally, feasibility studies have explored the incorporation of quantum entanglement into PET systems. For example, McNamara *et al.* [15], Eslami and Mohamadian [16], and Kim *et al.* [17] have proposed methods that leverage the quantum entanglement of annihilation photons to enhance imaging performance.

Initially, the focus was on the case in which each photon undergoes a single Compton scattering event [18,19]. The kinematics of this scenario have been simulated based on the theoretical work of Pryce and Ward [20] and Snyder *et al.* [21], who calculated the joint differential Compton scattering cross section while accounting for the effect of entanglement on the scattering distribution of the final annihilation photons; for brevity, this approach is referred to as the 2-Compton scattering theory. More recently, Caradonna [14] calculated the cross section for the case in which one photon undergoes two Compton scattering events while the other undergoes only one, an analysis referred to as the 3-Compton cross section, which has shown good agreement with recent experimental results [22,23].

Despite these advances, a systematic investigation of the physical properties of maximally entangled annihilation photons—especially their behavior following Compton scattering—remains incomplete. The present study aims to provide a theoretical framework to characterize the behavior and polarization properties of these photons under specific hypothetical conditions, which, in principle, can be conducted experimentally using Compton camera devices.

The polarization characteristics of an isolated annihilation photon beam are examined. This analysis establishes the definitions and relationships needed to describe the unpolarized state of a single beam, including the derivation of the

^{*}Contact author: petercaradonna65@gmail.com

differential scattering cross section using the Stokes vector formalism. Building on this foundation, a formulation is presented for the evolved density matrix of a two-photon system following Compton scattering. In this approach, the initial density matrix is transformed into a 4×4 Stokes density matrix. Compared with the method described in [14], this formulation allows for a more efficient calculation of the joint differential cross section for scenarios involving two or more Compton scattering events, and for analyzing the polarization state of each subsystem after a Compton interaction. Since this method is based on quantum field theory calculations [24], the results are expected to be consistent with traditional quantum field theory approaches.

This paper is organized as follows. Section II defines the polarization basis, introduces the Stokes vector formalism, and outlines the coordinate system and rotation conventions used in the analysis.

Section III analyzes the Compton scattering of a single annihilation photon beam. The results provide a reference model for interpreting polarization structure in the bipartite Stokes density matrix when applied to the investigation of the annihilation photons in Sec. V.

Section IV introduces the bipartite Stokes density matrix formalism, which enables the computation of the conditional Stokes vectors associated with each photon in a two-photon system and the joint scattering differential cross sections.

Section V examines the influence of entanglement on the polarization properties of two-photon annihilation states subjected to Compton scattering. The section introduces both entangled and classically correlated input states, formulates their Stokes density matrix representations, and applies the bipartite scattering framework to compute conditional polarization quantities. In addition, the conditional Stokes vectors are integrated over scattering angles to evaluate their behavior under averaging, establishing a basis for interpreting both postselected and trace-based measurements.

Finally, Sec. VI clarifies how the formalism captures conditional polarization effects without violating locality, and its potential use in PET imaging simulations is outlined. It emphasizes the distinction between postselected correlations and unchanged reduced states, and it highlights future directions for modeling entanglement in realistic scattering environments.

II. POLARIZATION CONVENTIONS

This section introduces the Stokes formalism as a geometrically intuitive and experimentally meaningful framework for describing polarization states relevant to Compton scattering. The mathematical structure of the Stokes representation is developed, including its connection to the circular polarization basis, its interpretation on the Poincaré sphere, and its transformation behavior under azimuthal rotations.

Photon polarization is expressed in the circular basis $\{|R\rangle, |L\rangle\}$, corresponding to right- and left-handed helicity eigenstates with spin projections $s_z = \pm 1$, as defined in Sec. II of Ref. [13]. An arbitrary pure state in this basis is written as

$$|\psi\rangle = c_1|R\rangle + c_2|L\rangle, \quad |c_1|^2 + |c_2|^2 = 1, \quad (1)$$

where $c_1, c_2 \in \mathbb{C}$ are probability amplitudes.

The polarization state $|\psi\rangle$ given in Eq. (1) can be equivalently described by a Stokes vector $|S\rangle$, defined using the expectation values of Pauli matrices σ_i ($i = 0, 1, 2, 3$):

$$|S\rangle = \begin{bmatrix} S_0 \\ S_1 \\ S_2 \\ S_3 \end{bmatrix} = \begin{bmatrix} \langle\psi|\sigma_0|\psi\rangle \\ \langle\psi|\sigma_1|\psi\rangle \\ \langle\psi|\sigma_2|\psi\rangle \\ \langle\psi|\sigma_3|\psi\rangle \end{bmatrix}. \quad (2)$$

The S_i parameters ($i = 0, 1, 2, 3$), given in Eq. (2), quantify physically measurable polarization differences. S_0 represents the total beam intensity. S_1 measures the difference in intensity between vertical and horizontal linear polarizations, S_2 is the difference between linear polarizations at $+45^\circ$ and -45° , and S_3 is the difference between right- and left-handed circular polarizations.

The degree of polarization p quantifies the purity of the beam and is given by

$$p = \frac{1}{S_0} \sqrt{S_1^2 + S_2^2 + S_3^2}, \quad 0 \leq p \leq 1. \quad (3)$$

A state is pure if $p = 1$, and mixed otherwise.

The Stokes parameters define a point inside or on the surface of the Poincaré sphere. Pure states lie on the surface; partially polarized (mixed) states lie inside. The poles represent circular polarizations ($S_3 = \pm 1$), the equator represents linear polarizations, and intermediate points describe elliptical polarization. Randomly polarized radiation corresponds to a point at the origin. This geometrical interpretation is illustrated in Fig. 1(a).

Figure 1(b) illustrates the coordinate system adopted in the laboratory frame. The coordinate axes x, y, z are chosen such that the momentum of the incident photon is aligned with the z -axis. The electric field vector lies in the xy -plane, and azimuthal rotations ϕ about the z -axis in general will transform the Stokes vector, since the Stokes parameters are dependent upon the choice of axes. In Stokes space, such a rotation corresponds to a transformation by an angle 2ϕ about the S_3 -axis [25]. This transformation is represented by the matrix

$$M(\phi) = \begin{bmatrix} 1 & 0 & 0 & 0 \\ 0 & \cos 2\phi & \sin 2\phi & 0 \\ 0 & -\sin 2\phi & \cos 2\phi & 0 \\ 0 & 0 & 0 & 1 \end{bmatrix}, \quad (4)$$

which performs a clockwise rotation about the S_3 -axis when viewed from above, as illustrated in Fig. 1(a). Since $M(\phi)$ is orthogonal, its inverse equals its transpose: $M(\phi)^{-1} = M(\phi)^\top$. Consequently, $M(-\phi) = M(\phi)^{-1} = M(\phi)^\top$, as required for reversible azimuthal rotations.

Using Eqs. (2) and (4), the transformed Stokes vector $|S'\rangle$ in the rotated coordinate frame is then

$$|S'\rangle = M(\phi)|S\rangle = \begin{bmatrix} S_0 \\ S_1 \cos 2\phi + S_2 \sin 2\phi \\ -S_1 \sin 2\phi + S_2 \cos 2\phi \\ -S_3 \end{bmatrix}, \quad (5)$$

where the sign of S_3 reflects the helicity convention adopted in [13] and in the particle physics literature more generally.

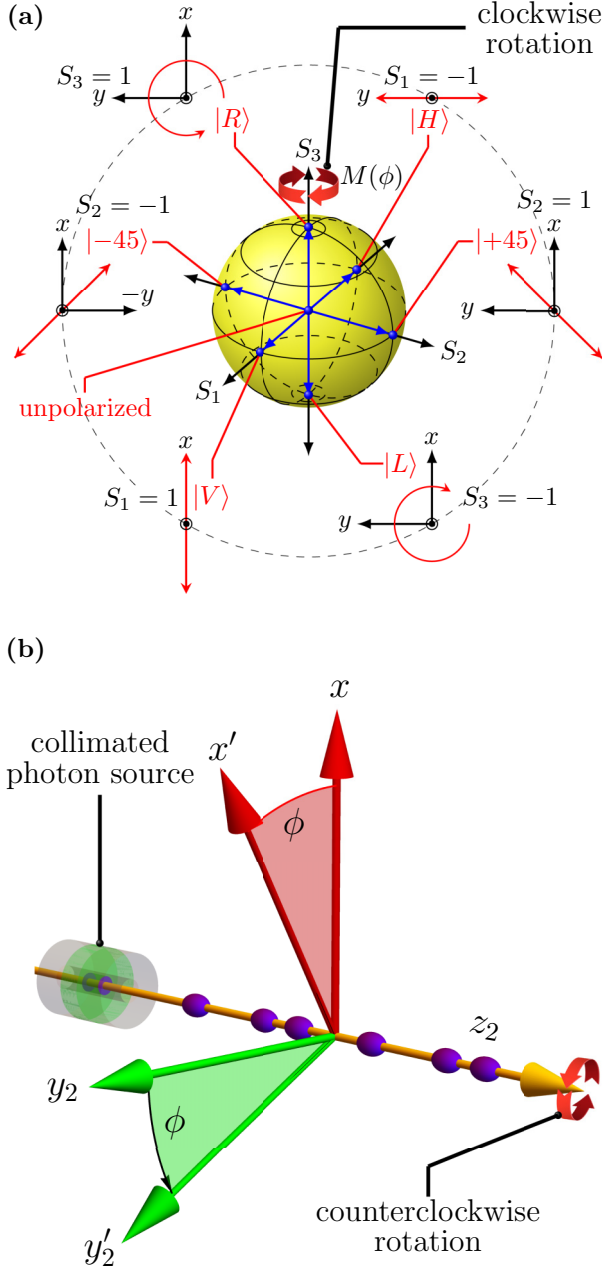


FIG. 1. (a) The Poincaré sphere illustrates various special cases of polarization states, with the matrix $M(\phi)$ representing a clockwise rotation by 2ϕ about the S_3 -axis when viewed from above. (b) The corresponding Euclidean geometry, where the Stokes vector represents the classical electric field vector in the xy -plane. A rotation of 2ϕ about the S_3 -axis corresponds to a counterclockwise rotation by ϕ in laboratory coordinates about z .

III. GEOMETRICAL AND POLARIZATION STRUCTURE OF A SCATTERED PHOTON

This section investigates the Compton scattering of a single annihilation photon beam. The analysis presented here establishes essential definitions and results for the single-photon case, which will be used in Sec. VB to interpret the polarization structure of the bipartite Stokes density matrix describing the two-photon annihilation system.

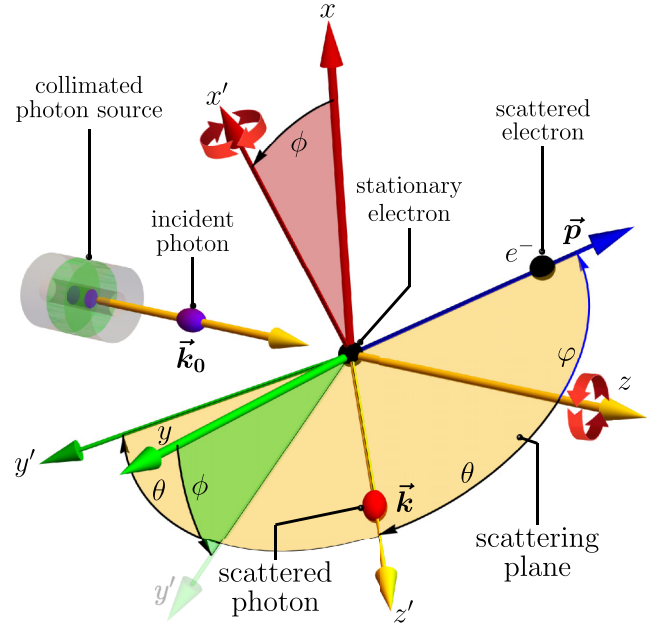


FIG. 2. Compton scattering: An incident photon with energy E_0 and momentum \vec{k}_0 strikes a stationary electron. Following the interaction, the electron recoils with total energy ϵ and momentum \vec{p} , subtending a polar angle ϕ with respect to \vec{k}_0 (the z -axis). The scattered photon emerges from the collision with energy $E(\theta)$, where θ is the scattering angle, and with momentum \vec{k} , oriented along the z' -axis. The scattering geometry of the photon can be modeled by a counterclockwise rotation about the z -axis by the angle ϕ followed by a clockwise rotation about the x' -axis by the angle θ .

Throughout this work, *natural units* are adopted, normalizing the electron mass m , the speed of light c , and the reduced Planck constant \hbar such that $m = c = \hbar = 1$. Consequently, the kinetic energy E_0 of incident photons from a monochromatic beam is expressed in units of mc^2 . For an incident beam of annihilation photons with kinetic energy mc^2 , this normalization yields $E_0 = 1$.

Figure 2 depicts a hypothetical experiment designed to isolate and study one of the annihilation beams produced from a positron-emitting source. In this experiment, positrons are assumed to annihilate with electrons at rest in a net spin-zero configuration. This setup results in the emission of predominantly two photons in a back-to-back configuration, each with an incident kinetic energy of $E_0 = 1$. A collimator ensures that only photons emitted along the z -axis are transmitted.

As shown in Sec. VB, Eq. (23), the isolated annihilation beams are unpolarized. Accordingly, the Stokes vector $|\hat{S}\rangle$ describing a single incident annihilation beam takes the standard form for an unpolarized source such that

$$|\hat{S}\rangle = \begin{bmatrix} 1 \\ 0 \\ 0 \\ 0 \end{bmatrix},$$

where the hat indicates normalization with respect to total beam intensity, such that $S_0 = 1$.

Figure 2 depicts an incident annihilation photon with linear momentum $\vec{k}_0 = E_0/c\hat{z} = \hat{z}$ (in natural units), propagating toward the origin of a Cartesian coordinate system defined by $\{x, y, z\}$. Upon impact, it is assumed that the photon interacts with a stationary electron whose spin is randomly aligned with respect to the laboratory frame. The kinetic energy of the scattered photon $E(\theta)$ is given by the Compton relation

$$E(\theta) = \frac{1}{2 - \cos \theta}, \quad (\text{in units of } mc^2),$$

where θ is the scattering angle between the momenta of the incident and scattered photons.

The linear momentum \vec{k} of the scattered photon, expressed in terms of θ and ϕ , is given by

$$\vec{k} = -\frac{\sin \theta \sin \phi}{2 - \cos \theta} \hat{x} + \frac{\sin \theta \cos \phi}{2 - \cos \theta} \hat{y} + \frac{\cos \theta}{2 - \cos \theta} \hat{z}.$$

By conservation of energy, the kinetic energy ϵ of the recoiling electron is

$$\epsilon = 1 - E(\theta) = \frac{1 - \cos \theta}{2 - \cos \theta}.$$

Neglecting the work function of the scattering medium, the magnitude of the electron momentum is

$$|\vec{p}| = \sqrt{\epsilon(\epsilon + 2)} = \sqrt{\frac{3 \cos^2 \theta - 8 \cos \theta + 5}{(2 - \cos \theta)^2}},$$

with explicit vector form given by

$$\vec{p} = \frac{\sin \theta \sin \phi}{2 - \cos \theta} \hat{x} - \frac{\sin \theta \cos \phi}{2 - \cos \theta} \hat{y} + \frac{2(1 - \cos \theta)}{2 - \cos \theta} \hat{z}.$$

Alternatively, by combining energy and momentum conservation, the electron momentum vector may be written in terms of the polar angle φ it makes with the z -axis:

$$\vec{p} = \sqrt{\epsilon(\epsilon + 2)}(\sin \varphi \sin \phi \hat{x} - \sin \varphi \cos \phi \hat{y} + \cos \varphi \hat{z}).$$

In the scattering frame $\{x', y', z'\}$, the relevant momenta are

$$\vec{k}_0 = -E_0 \sin \theta \hat{y}' + E_0 \cos \theta \hat{z}',$$

$$\vec{k} = E(\theta) \hat{z}',$$

$$\vec{p} = \sqrt{\epsilon(\epsilon + 2)}(-\sin(\theta + \varphi) \hat{y}' + \cos(\theta + \varphi) \hat{z}').$$

In this convention, photon momentum vectors always lie along the z - or z' -axes of their respective frames. The transformation from $\{x, y, z\}$ to $\{x', y', z'\}$ is performed via a counterclockwise rotation about z by angle ϕ , followed by a clockwise rotation about x' by angle θ , as shown in Fig. 2. The x' -axis lies in the xy plane, and the y' - z' plane defines the scattering plane, containing both the scattered photon and electron.

The objective here is to elucidate how these Euclidean rotations transform the initial Stokes vector $|\hat{S}\rangle$ into the final polarization state $|\hat{S}'\rangle$ of the scattered photon, whose electric field is confined to the $x'y'$ plane. This transformation is modeled by a 4×4 Mueller matrix $T(\theta)$. For an unpolarized electron target, the Mueller matrix $T_{\text{un}}(\theta)$ takes the form

[Eq. (28) of Ref. [13]]

$$T_{\text{un}}(\theta) = \frac{r_o^2}{2} \left(\frac{E(\theta)}{E_0} \right)^2 \begin{bmatrix} t_{11} & t_{12} & 0 & 0 \\ t_{12} & 2 - t_{12} & 0 & 0 \\ 0 & 0 & t_{33} & 0 \\ 0 & 0 & 0 & t_{44} \end{bmatrix}. \quad (6)$$

This matrix is symmetric such that $T_{\text{un}}(\theta) = T_{\text{un}}^\top(\theta)$. The elements t_{mn} are real-valued functions of θ , with explicit forms:

$$\begin{aligned} t_{11} &= \frac{\cos \theta (\cos^2 \theta - 3 \cos \theta + 3) - 3}{\cos \theta - 2}, \\ t_{12} &= \sin^2 \theta, \\ t_{33} &= 2 \cos \theta, \\ t_{44} &= \frac{\cos \theta [\cos \theta (4 - \cos \theta) - 5]}{\cos \theta - 2}. \end{aligned} \quad (7)$$

Using Eqs. (5) and (6), the transition from $|\hat{S}\rangle \mapsto |\hat{S}'\rangle$ of an unpolarized annihilation beam Compton scattering off an unpolarized scattering medium is given by the matrix equation

$$|\hat{S}'\rangle = T_{\text{un}}(\theta) M(\phi) |\hat{S}\rangle = \frac{r_o^2}{2} \left(\frac{E(\theta)}{E_0} \right)^2 t_{11} |\hat{S}'\rangle,$$

where

$$|\hat{S}'\rangle = \begin{bmatrix} 1 \\ \frac{t_{12}}{t_{11}} \\ 0 \\ 0 \end{bmatrix} = \begin{bmatrix} 1 \\ p' \\ 0 \\ 0 \end{bmatrix}. \quad (8)$$

Using Eq. (3), it can be shown that the quantity t_{12}/t_{11} is the degree of polarization of the scattered beam and is denoted as p' . Using the definitions for t_{11} and t_{12} given in Eqs. (7), it can be shown that

$$\begin{aligned} p' &= \frac{t_{12}}{t_{11}}, \\ p' &= \frac{(\cos \theta - 2) \sin^2 \theta}{\cos \theta (3 - 3 \cos \theta + \cos^2 \theta) - 3}. \end{aligned} \quad (9)$$

Figure 3 shows the degree of polarization p' of the scattered beam, defined in Eq. (9).

Figure 4 schematically illustrates the effect of Compton scattering on the polarization state of an initially unpolarized beam in Poincaré space.

The spectral decomposition of the scattered beam can be found by transforming the Stokes vector $|\hat{S}'\rangle$ into the density matrix ρ' whose spectral elements belong to the Hilbert space of states. Using the method of Abouraddy *et al.* [26], the spectral decomposition of ρ' can be described by the equation

$$\rho' = \frac{1}{2} \sum_{i=0}^3 S'_i \sigma_i = I_v |V'\rangle \langle V'| + I_h |H'\rangle \langle H'|, \quad (10)$$

where σ_i are the Pauli matrices. The basis state $|V'\rangle$ corresponds to vertical polarization, oriented orthogonal to the scattering plane and aligned with the x' -axis, while $|H'\rangle$ denotes horizontal polarization, lying within the scattering plane

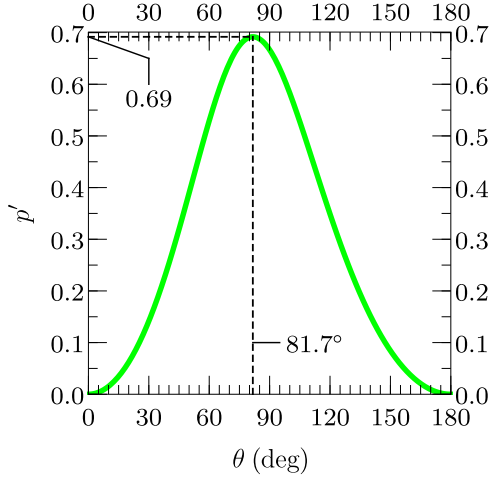


FIG. 3. The degree of polarization of the scattered beam, resulting from an initially unpolarized 511 keV photon beam, is shown in Fig. 2 as a function of the Compton scattering angle θ . It reaches a maximum value of 0.69 at $\theta = 81.7^\circ$.

and aligned along the y' -axis. The basis states in Eq. (10) are defined as

$$|V'\rangle = \frac{1}{\sqrt{2}} \begin{bmatrix} 1 \\ 1 \end{bmatrix}, \quad |H'\rangle = \frac{1}{\sqrt{2}} \begin{bmatrix} 1 \\ -1 \end{bmatrix}. \quad (11)$$

The fractional beam intensities $I_{v'}$ and $I_{h'}$ defined in Eq. (10) can be expressed in terms of the degree of polarization

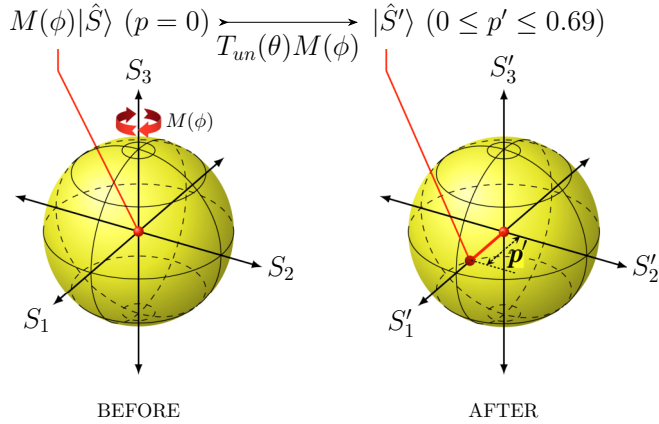


FIG. 4. BEFORE: An azimuthal rotation about the z -axis by an angle ϕ (as shown in Fig. 2) corresponds to a clockwise rotation about the S_3 -axis in Poincaré space, as viewed from the positive S_3 direction toward the origin. For an initially unpolarized beam ($p = 0$), applying the rotation matrix $M(\phi)$ to the Stokes vector $|\hat{S}\rangle$ leaves the vector unchanged, i.e., $M(\phi)|\hat{S}\rangle = |\hat{S}\rangle$, indicating rotational symmetry, as expected for an unpolarized beam. AFTER: In contrast, Compton scattering by an angle θ alters the magnitude of the Stokes vector, corresponding to a change in the degree of polarization p' of the scattered beam (see also Fig. 3). The resulting Stokes vector is aligned along the positive S'_1 axis, indicating that the beam becomes partially polarized in the vertical direction relative to the scattering plane. Since $p' < 1$, it indicates a mixed final state.

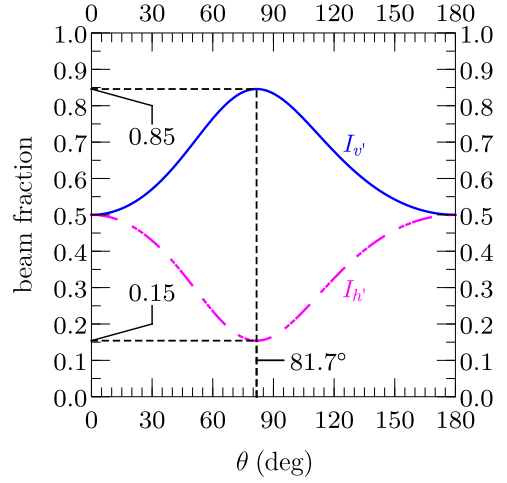


FIG. 5. The normalized scattered beam intensities, $I_{v'}$ and $I_{h'}$, represent the fractions of vertically $|V'\rangle$ and horizontally $|H'\rangle$ polarized photons, respectively, relative to the scattering plane for an initial source of 511 keV unpolarized incident photons. The intensities of these two components are plotted as functions of the scattering angle θ .

tion p' from Eq. (9) as

$$I_{v'} = \frac{1 + p'}{2}, \quad I_{h'} = \frac{1 - p'}{2}. \quad (12)$$

The coefficients $I_{v'}$ and $I_{h'}$ represent the probabilities of measuring a scattered photon in the $|V'\rangle$ or $|H'\rangle$ states, respectively. Using Eqs. (10) and (11), we find that

$$I_{v'} = \langle V' | \rho' | V' \rangle, \quad I_{h'} = \langle H' | \rho' | H' \rangle.$$

Figure 5 shows the normalized intensity fractions $I_{v'}$ and $I_{h'}$, defined in Eq. (12), which represent the proportions of the beam in the $|V'\rangle$ and $|H'\rangle$ polarization states, respectively, as functions of the scattering angle θ . These intensities satisfy the normalization condition $I_{v'} + I_{h'} = 1$ for all angles. For an initially unpolarized beam, the results are independent of the azimuthal angle ϕ , consistent with rotational symmetry about the propagation axis. The plots demonstrate that Compton scattering acts as a polarization filter, preferentially enhancing vertical polarization while suppressing horizontal polarization relative to the scattering plane. The figure also illustrates the probabilistic nature of this filtering process: for annihilation photons, the likelihood of detecting a vertically polarized photon can approach—but never exceed—85% certainty.

The absolute probability of Compton scattering of an incident annihilation photon in the direction of the z' -axis is described by the differential Compton scattering cross section $d\sigma/d\Omega$. For annihilation photons with wavelengths of 2.4×10^{-12} m, polarization filters that can discriminate between the $|V'\rangle$ and $|H'\rangle$ states of the scattered beam are not available. Therefore, polarization-insensitive detectors are employed. Within the Stokes framework, these detectors are characterized by the Stokes vector $\langle I \rangle = [1, 0, 0, 0]$ (Ref. [14], Appendix B). For a beam of unpolarized annihilation photons scattering off unpolarized electrons, the differential cross

section can be computed as follows:

$$\begin{aligned} \frac{d\sigma}{d\Omega} &= \langle I | T_{\text{un}}(\theta) M(\phi) | \hat{S} \rangle \\ &= \frac{r_0^2}{2} \frac{\cos \theta [\cos \theta (\cos \theta - 3) + 3] - 3}{(\cos \theta - 2)^3}. \end{aligned} \quad (13)$$

IV. BIPARTITE STOKES DENSITY MATRIX

A. Single Compton scattering

Consider a general 4×4 density matrix ρ describing a two-photon system in the Hilbert space $\mathcal{H} = \mathcal{H}_1 \otimes \mathcal{H}_2$, where \mathcal{H}_1 and \mathcal{H}_2 correspond to subsystem 1 and 2, respectively. The matrix ρ can be symbolically represented as

$$\rho = \begin{bmatrix} \rho_{11} & \rho_{12} & \rho_{13} & \rho_{14} \\ \rho_{12}^* & \rho_{22} & \rho_{23} & \rho_{24} \\ \rho_{13}^* & \rho_{23}^* & \rho_{33} & \rho_{34} \\ \rho_{14}^* & \rho_{24}^* & \rho_{34}^* & \rho_{44} \end{bmatrix},$$

where ρ is expressed in the operational basis $|R, R\rangle, |R, L\rangle, |L, R\rangle, |L, L\rangle$, ordered from top to bottom and left to right, Hermiticity is ensured by the condition $\rho = \rho^\dagger$, and where normalization is enforced by the trace condition $\text{Tr}[\rho] = 1$.

Following the method introduced by Abouraddy *et al.* [26], the density matrix ρ can be mapped to a real-valued 4×4 matrix of Stokes parameters via

$$S_{ij} = \text{Tr}[(\sigma_i \otimes \sigma_j) \rho], \quad i, j = 0, 1, 2, 3, \quad (14)$$

where σ_0 is the identity and $\sigma_1, \sigma_2, \sigma_3$ are the Pauli matrices. While this decomposition has been employed in optical systems, the present formulation applies it to Compton scattering, where the Stokes parameters are explicitly organized into this operator basis. The resulting matrix S , referred to here as the Stokes density matrix, is given by

$$\rho \mapsto S = \begin{bmatrix} S_{00} & S_{01} & S_{02} & S_{03} \\ S_{10} & S_{11} & S_{12} & S_{13} \\ S_{20} & S_{21} & S_{22} & S_{23} \\ S_{30} & S_{31} & S_{32} & S_{33} \end{bmatrix}. \quad (15)$$

The individual Stokes vectors $|S_1\rangle$ and $|S_2\rangle$ for subsystems 1 and 2 can be extracted directly from the first column and row of S where

$$|S_1\rangle = \begin{bmatrix} S_{00} \\ S_{10} \\ S_{20} \\ S_{30} \end{bmatrix}, \quad |S_2\rangle = \begin{bmatrix} S_{00} \\ S_{01} \\ S_{02} \\ S_{03} \end{bmatrix}. \quad (16)$$

From these components, the conditional reduced density matrices for the idler and signal photons are given by

$$\rho_1 = \frac{1}{2S_{00}} \begin{bmatrix} S_{00} + S_{30} & S_{10} - iS_{20} \\ S_{10} + iS_{20} & S_{00} - S_{30} \end{bmatrix}, \quad (17a)$$

$$\rho_2 = \frac{1}{2S_{00}} \begin{bmatrix} S_{00} + S_{03} & S_{01} - iS_{02} \\ S_{01} + iS_{02} & S_{00} - S_{03} \end{bmatrix}. \quad (17b)$$

The interpretation of these as conditional reduced density matrices will be revisited in Sec. VD, where the formalism is applied to the specific case of annihilation photon scattering, and further elaborated in the Conclusion (Sec. VI).

Using the definition of the degree of polarization from Eq. (3), the polarization/purities p_1 and p_2 of the respective subsystems are given by

$$\begin{aligned} p_1 &= \frac{1}{S_{00}} \sqrt{S_{10}^2 + S_{20}^2 + S_{30}^2}, \\ p_2 &= \frac{1}{S_{00}} \sqrt{S_{01}^2 + S_{02}^2 + S_{03}^2}. \end{aligned} \quad (18)$$

If only subsystem 1 undergoes Compton scattering at polar and azimuthal angles θ_1 and ϕ_1 , respectively, the transformed Stokes matrix S'_1 is described by the ansatz

$$S'_1 = T_{\text{un}}(\theta_1) M(\phi_1) S.$$

Conversely, if only subsystem 2 scatters, the evolved Stokes matrix S'_2 is given by the ansatz

$$S'_2 = S M^\top(\phi_2) T_{\text{un}}^\top(\theta_2) = S M(-\phi_2) T_{\text{un}}(\theta_2). \quad (19)$$

B. Multiple Compton scattering

Assuming that dispersion effects remain negligible for each photon wave packet throughout m and n scattering events, the cumulative effect of all $m + n$ interactions is captured by the transformed Stokes matrix

$$S^{(m,n)} = \left(\prod_{j=m}^1 T_{1j} M_{1j} \right) S \left(\prod_{j=n}^1 T_{2j} M_{2j} \right)^\top, \quad (20)$$

where \prod denotes the product operator, and T_{pj} and M_{pj} represent the Compton scattering Mueller matrix and azimuthal rotation matrix, respectively, for the j th scattering event experienced by photon $p = 1, 2$. The index $j = 1$ corresponds to the first interaction, while $j = m$ or n denotes the final interaction registered in coincidence.

The Mueller matrix T_{pj} represents the general form of the Compton interaction matrix, with its functional expression given in Eq. (43) of [14] and matrix elements listed in Table 2. The corresponding rotation matrices M_{pj} , defined in Eq. (45) of the same reference, implement Stokes-space rotations by an angle $2\phi_{pj}$ about the S_3 axis. A schematic depiction of the complete (m, n) scattering configuration is provided in Fig. 2 of [14].

In the absence of scattering events ($m = n = 0$), the matrices are defined as

$$T_{p0} = M_{p0} := \mathbb{I}_4,$$

where \mathbb{I}_4 is the 4×4 identity matrix.

Using Eq. (20), the absolute joint differential cross section for the coincident detection of scattered photons following the m th and n th scattering events is given by

$$\frac{d^2\sigma}{d\Omega_1 d\Omega_2} = \frac{1}{4} \langle I_1 | S^{(m,n)} | I_2 \rangle, \quad (21)$$

where $d\Omega_1, d\Omega_2$ denote the solid angles subtended by the detectors. This expression assumes that a pair of detectors operates in coincidence mode.

V. ENTANGLED VERSUS SEPARABLE STATES

A. Introduction

The entangled annihilation photon state with concurrence $\mathcal{C} = 1$ is contrasted with a hypothetical model that preserves the polarization correlations of the Bell state but is represented by a mixed state with concurrence $\mathcal{C} = 0$. Originally proposed by Bohm and Aharonov [27,28], this model reproduces the polarization statistics of the entangled case while remaining entirely separable.

In the Bohm-Aharonov mixed state, spin angular momentum is not conserved in individual scattering events relative to a fixed axis, unlike the Bell state [13]. However, as discussed in [27], conservation holds on average, consistent with experimental observations of annihilation photons. As a result, the mixed state exhibits the same rotational symmetry about the propagation axis as the maximally entangled case.

B. Initial-state construction and symmetry in Stokes space

Consider a two-photon system resulting from the annihilation of an electron-positron pair with opposite spins at rest. Each photon, with a kinetic energy of 511 keV, propagates in opposite directions to conserve linear momentum. The maximally entangled Bell state representing this system, denoted $|\psi_c^-\rangle$ in the circular polarization basis and its linear polarization basis equivalent $|\psi_l^+\rangle$, is detailed in [13], along with its associated density matrix ρ_{en} . A key novel result of this work is the application of Eqs. (14) and (15) to transform ρ_{en} into its Stokes density matrix representation such that

$$\rho_{\text{en}} \longrightarrow S(\rho_{\text{en}}) = \begin{bmatrix} 1 & 0 & 0 & 0 \\ 0 & -1 & 0 & 0 \\ 0 & 0 & 1 & 0 \\ 0 & 0 & 0 & 1 \end{bmatrix}. \quad (22)$$

As with ρ_{en} , the corresponding Stokes matrix $S(\rho_{\text{en}})$ is symmetric, satisfying $S(\rho_{\text{en}}) = S^T(\rho_{\text{en}})$.

Applying the rule defined in Eq. (16), the unit Stokes vectors for subsystems 1 and 2 can be extracted from the Stokes matrix in Eq. (22). They are given explicitly by

$$|\hat{S}_1(\rho_{\text{en}})\rangle = |\hat{S}_2(\rho_{\text{en}})\rangle = \begin{bmatrix} 1 \\ 0 \\ 0 \\ 0 \end{bmatrix}. \quad (23)$$

Let $p_{\text{en}}^{(1)}$ and $p_{\text{en}}^{(2)}$ denote the degree of polarization for subsystem 1 and 2, respectively. Using Eq. (18), we find that $p_{\text{en}}^{(1)} = p_{\text{en}}^{(2)} = 0$, indicating that the two bidirectional beams are initially unpolarized, as expected.

Using Eq. (17), the Stokes vectors in Eq. (23) can be mapped to 2×2 reduced density matrices in Hilbert space, denoted $\rho_{\text{en}}^{(1)}$ and $\rho_{\text{en}}^{(2)}$ for subsystems 1 and 2, respectively. These matrices admit a spectral decomposition in the linear polarization basis $|V\rangle, |H\rangle$ such that

$$\begin{aligned} \rho_{\text{en}1} &= \frac{1}{2}|V_1\rangle\langle V_1| + \frac{1}{2}|H_1\rangle\langle H_1| = \frac{1}{2}\mathbb{I}_2, \\ \rho_{\text{en}2} &= \frac{1}{2}|V_2\rangle\langle V_2| + \frac{1}{2}|H_2\rangle\langle H_2| = \frac{1}{2}\mathbb{I}_2. \end{aligned} \quad (24)$$

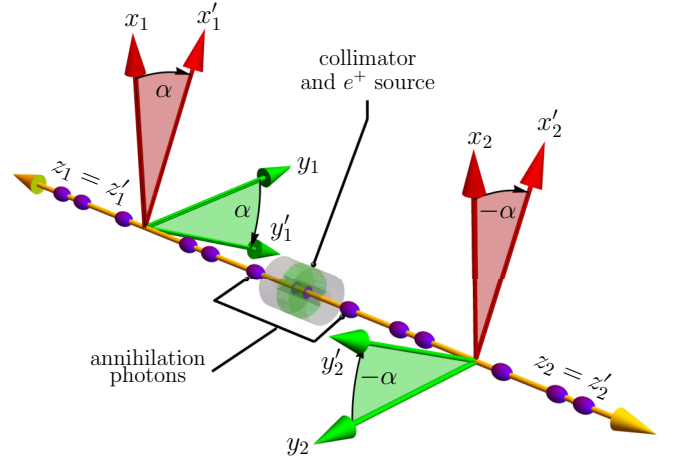


FIG. 6. A simple illustration depicts the coupled counter-rotation of a bidirectional beam of 511 keV photons in the state $|\psi_l^+\rangle$ [Ref. [13], Eq. (21)]. The rotation is viewed from the positive z -axis towards the origin. The beams are collimated to propagate along both the positive and negative z -axis. A counter-rotation of the coordinate system around the propagation axis by an azimuthal angle α is applied. Due to the rotational symmetry of the quantum state $|\psi_c^-\rangle$, this rotation leaves both the state and its associated Stokes density matrix $S(\rho_{\text{en}})$ unchanged [see Eq. (34)].

where \mathbb{I}_2 denotes the 2×2 identity matrix. This indicates that each beam corresponds to an equal incoherent mixture of vertical and horizontal polarization states.

The cross-polarization correlation relationship of $|\psi_l^+\rangle$ remains invariant under a coupled rotation of the coordinate systems around the propagation axis by an azimuthal angle α , as illustrated in Fig. 6 [13,27]. In Stokes space, this corresponds to a clockwise rotation by an angle α about the S_{30} axis for subsystem 1. Simultaneously, it corresponds to a counterclockwise rotation about the S_{03} axis for subsystem 2. This transformation can be mathematically expressed as

$$S(\rho_{\text{en}}) = M(\alpha)S(\rho_{\text{en}})M(\alpha). \quad (25)$$

With the z -axis aligned parallel to the beam propagating, Eq. (25) implies that one is free to choose any orientation α for the x - and y -axis. This freedom arises from the rotational symmetry of the state $|\psi_l^+\rangle$ with respect to the propagation axis [13,27].

In contrast, the Bohm-Aharonov mixed state (ρ_{ls}) is constructed as an ensemble average over all cross-polarization orientations, defined explicitly in [13]. Its transformation into Stokes space is given by

$$\rho_{\text{ls}} \longrightarrow S(\rho_{\text{ls}}) = \begin{bmatrix} 1 & 0 & 0 & 0 \\ 0 & -\frac{1}{2} & 0 & 0 \\ 0 & 0 & \frac{1}{2} & 0 \\ 0 & 0 & 0 & 0 \end{bmatrix}, \quad (26)$$

which is symmetric.

The corresponding unit Stokes vectors for subsystems 1 and 2 of the Bohm-Aharonov mixed state, derived using the

same procedure in obtaining Eq. (23), are given by

$$|\hat{S}_1(\rho_{ls})\rangle = |\hat{S}_2(\rho_{ls})\rangle = \begin{bmatrix} 1 \\ 0 \\ 0 \\ 0 \end{bmatrix}. \quad (27)$$

As with the unit Stokes vectors $|\hat{S}_1(\rho_{en})\rangle$ and $|\hat{S}_2(\rho_{en})\rangle$ in Eq. (23), the vectors $|\hat{S}_1(\rho_{ls})\rangle$ and $|\hat{S}_2(\rho_{ls})\rangle$ in Eq. (27) also represent unpolarized beams. This outcome reflects the construction of ρ_{ls} and confirms that the Stokes vectors for both subsystems in the mixed state are mathematically identical to those in the entangled state. Therefore,

$$|\hat{S}_1(\rho_{ls})\rangle = |\hat{S}_1(\rho_{en})\rangle = |\hat{S}_2(\rho_{ls})\rangle = |\hat{S}_2(\rho_{en})\rangle.$$

It follows that the reduced density matrices for subsystems 1 and 2 of ρ_{ls} , denoted ρ_{ls_1} and ρ_{ls_2} , have spectral decompositions identical to those of ρ_{en_1} and ρ_{en_2} , given in Eqs. (24):

$$\rho_{ls_1} = \rho_{en_1}, \quad \rho_{ls_2} = \rho_{en_2}.$$

In analogy with $S(\rho_{en})$, the Stokes matrix $S(\rho_{ls})$ remains invariant under a coupled rotation of the coordinate systems about the propagation axis by an azimuthal angle α [see Eq. (25)]. Accordingly, it satisfies the relation

$$S(\rho_{ls}) = M(\alpha)S(\rho_{ls})M(\alpha). \quad (28)$$

C. Reformulation of 2- and 3-Compton scattering

Using the Compton scattering ansatz introduced in Sec. IV A, together with Eq. (21), the joint differential cross section for the 2-Compton scattering configuration is given by

$$\frac{d^2\sigma}{d\Omega_{11}d\Omega_{21}} = \frac{1}{4} \langle I_1 | S^{(1,1)}(\rho_{en}) | I_2 \rangle, \quad (29)$$

where

$$S^{(1,1)}(\rho_{en}) = T_{11}M_{11}S(\rho_{en})M_{21}^\top T_{21}^\top.$$

For the 3-Compton scattering case—where one photon (taken without loss of generality to be the photon associated with subsystem 2) undergoes two successive scattering events while the other undergoes one—the corresponding cross section is given by

$$\frac{d^2\sigma}{d\Omega_{11}d\Omega_{22}} = \frac{1}{4} \langle I_1 | S^{(1,2)}(\rho_{en}) | I_2 \rangle, \quad (30)$$

where

$$S^{(1,2)}(\rho_{en}) = T_{11}M_{11}S(\rho_{en})M_{21}^\top T_{21}^\top M_{22}^\top T_{22}^\top.$$

Equations (29) and (30) recast the 2-Compton and 3-Compton scattering configurations—originally developed in [20] and [14], respectively—in a generalized bipartite Stokes matrix framework.

D. Evolved Stokes vectors under single-subsystem interaction

When both subsystems 1 and 2 are involved in Compton scattering, the angular variables θ and ϕ are typically labeled with subscripts 1 and 2 to distinguish the scattering geometries of the respective subsystems. In this study, subsystem 2 is arbitrarily selected to undergo Compton scattering in order to examine how such an interaction influences the polarization characteristics of both photon beams. The choice of subsystem is inconsequential, as the results are expected to remain symmetric: in the center-of-mass frame and on an event-by-event basis, the two annihilation photons possess identical kinetic energy and are detected with correlated polarizations, either both right- or both left-circularly polarized. Since only one subsystem is considered to scatter, the subscript indices on θ and ϕ are dropped, and it is to be understood that these angles refer exclusively to the local coordinate system of subsystem 2.

The photon associated with subsystem 2, which interacts with an unpolarized electron medium, will henceforth be referred to as the “signal photon.” Conversely, the photon associated with subsystem 1, which does not interact with the medium, will be referred to as the “idler photon.”

Let $S'(\rho_{en})$ denote the Stokes density matrix that evolves from the initial state $S(\rho_{en})$ in Eq. (22) as a result of a Compton scattering event involving the signal photon. Using the rightmost expression in Eq. (19) (Sec. IV A), the evolved matrix is given by

$$S'(\rho_{en}) = S(\rho_{en})M(-\phi)T_{un}(\theta). \quad (31)$$

As shown in Sec. IV B, the Stokes density matrix $S(\rho_{en})$ is invariant under a coupled rotation of the coordinate systems. Exploiting this invariance, we substitute the expression for $S(\rho_{en})$ in Eq. (25) into Eq. (31), which yields

$$S'(\rho_{en}) = M(\alpha)S(\rho_{en})M(\alpha)M(-\phi)T_{un}(\theta). \quad (32)$$

Equating the right-hand sides of Eqs. (31) and (32) yields the identity

$$S(\rho_{en})M(-\phi)T_{un}(\theta) = M(\alpha)S(\rho_{en})M(\alpha - \phi)T_{un}(\theta), \quad (33)$$

where the composition property of rotation matrices $M(x)M(y) = M(x + y)$ has been used.

Since we are free to choose any value for α , we can set $\alpha = \phi$, which implies $\alpha - \phi = 0$ and therefore $M(0) = \mathbb{I}_4$. Equation (33) then reduces to

$$S'(\rho_{en}) = S(\rho_{en})M(-\phi)T_{un}(\theta) = M(\phi)S(\rho_{en})T_{un}(\theta). \quad (34)$$

The geometrical interpretation of the expression given on the left- and right-hand side of Eq. (34) is illustrated in Figs. 7(a) and 7(b), respectively.

Using Eqs. (4) and (6), it can be shown, for the case of $S'(\rho_{en})$, that Eq. (31) evaluates to

$$S'(\rho_{en}) = \frac{r_o^2}{2} \left(\frac{E(\theta)}{E_0} \right)^2 \times \begin{bmatrix} t_{11} & t_{12} & 0 & 0 \\ -t_{12} \cos 2\phi & -(2 - t_{12}) \cos 2\phi & t_{33} \sin 2\phi & 0 \\ t_{12} \sin 2\phi & (2 - t_{12}) \sin 2\phi & t_{33} \cos 2\phi & 0 \\ 0 & 0 & 0 & t_{44} \end{bmatrix}. \quad (35a)$$

Additionally, since the Bohm and Aharonov mixed state ρ_{ls} exhibits the same invariance under a coupled rotation of the coordinate systems, the results derived for the entangled state using Eqs. (31)–(34) also apply to $S'(\rho_{ls})$.

Substituting $S(\rho_{\text{en}})$ in Eq. (31) with $S(\rho_{\text{ls}})$, the corresponding evolved Stokes density matrix $S'(\rho_{\text{ls}})$ has the following form:

$$S'(\rho_{\text{ls}}) = \frac{r_o^2}{2} \left(\frac{E(\theta)}{E_0} \right)^2 \times \begin{bmatrix} t_{11} & t_{12} & 0 & 0 \\ -\frac{1}{2}t_{12} \cos 2\phi & -\frac{1}{2}(2 - t_{12}) \cos 2\phi & \frac{1}{2}t_{33} \sin 2\phi & 0 \\ \frac{1}{2}t_{12} \sin 2\phi & \frac{1}{2}(2 - t_{12}) \sin 2\phi & \frac{1}{2}t_{33} \cos 2\phi & 0 \\ 0 & 0 & 0 & 0 \end{bmatrix}. \quad (35b)$$

The evolved Stokes vectors for the idler ($|S'_i\rangle$) and signal ($|S'_s\rangle$) beams, corresponding to the entangled state $S'(\rho_{\text{en}})$ and the Bohm-Aharonov mixed state $S'(\rho_{\text{ls}})$, can be expressed symbolically as

$$\begin{aligned} |S'_i(\rho_{\text{en}})\rangle &= t_{11} \frac{r_o^2}{2} \left(\frac{E(\theta)}{E_0} \right)^2 |\hat{S}'_i(\rho_{\text{en}})\rangle, \\ |S'_s(\rho_{\text{en}})\rangle &= t_{11} \frac{r_o^2}{2} \left(\frac{E(\theta)}{E_0} \right)^2 |\hat{S}'_s(\rho_{\text{en}})\rangle, \end{aligned} \quad (36a)$$

and

$$\begin{aligned} |S'_i(\rho_{\text{ls}})\rangle &= t_{11} \frac{r_o^2}{2} \left(\frac{E(\theta)}{E_0} \right)^2 |\hat{S}'_i(\rho_{\text{ls}})\rangle, \\ |S'_s(\rho_{\text{ls}})\rangle &= t_{11} \frac{r_o^2}{2} \left(\frac{E(\theta)}{E_0} \right)^2 |\hat{S}'_s(\rho_{\text{ls}})\rangle. \end{aligned} \quad (36b)$$

In formulating this theory, an apparent ambiguity arises regarding which Stokes vector in Eqs. (35a) and (35b)—the first column or the first row—corresponds to the signal or idler photon beams. This ambiguity can be resolved by referencing the single-beam analysis in Sec. III, where the final Stokes vector derived in Eq. (8) is associated with the signal beam. Based on this correspondence, the first row in Eqs. (35a) and (35b) defines the polarization characteristics of the signal beam. Consequently, the first column represents the polarization characteristics of the idler beam.

As a result of this identification process, the normalized Stokes vectors of the idler beam $|\hat{S}'_i(\rho_{\text{en}})\rangle$ and signal beam $|\hat{S}'_s(\rho_{\text{en}})\rangle$ symbolically introduced in Eq. (36a) for the initially entangled state ρ_{en} are explicitly defined as

$$|\hat{S}'_i(\rho_{\text{en}})\rangle = \begin{bmatrix} 1 \\ -p' \cos(2\phi) \\ p' \sin(2\phi) \\ 0 \end{bmatrix}, \quad |\hat{S}'_s(\rho_{\text{en}})\rangle = \begin{bmatrix} 1 \\ p' \\ 0 \\ 0 \end{bmatrix}. \quad (37a)$$

Likewise, the normalized Stokes vectors of the idler beam $|\hat{S}'_i(\rho_{\text{ls}})\rangle$ and signal beam $|\hat{S}'_s(\rho_{\text{ls}})\rangle$ symbolically introduced in Eq. (36b) for the Bohm-Aharonov mixed state ρ_{ls} are explicitly defined as

$$|\hat{S}'_i(\rho_{\text{ls}})\rangle = \begin{bmatrix} 1 \\ -\frac{1}{2}p' \cos(2\phi) \\ \frac{1}{2}p' \sin(2\phi) \\ 0 \end{bmatrix}, \quad |\hat{S}'_s(\rho_{\text{ls}})\rangle = \begin{bmatrix} 1 \\ p' \\ 0 \\ 0 \end{bmatrix}, \quad (37b)$$

where the quantity p' is the degree of polarization discussed in Sec. III, Eq. (9), and Fig. 3 for the case of the single beam analysis.

As shown in Eqs. (37a) and (37b), the S_3 Stokes parameters are zero, meaning that the state space of the Stokes vectors

for both the idler and signal beams after a Compton interaction are confined to the equatorial plane of the Poincaré sphere, as illustrated in Fig. 8. The direction of the Stokes vector for the idler beam, in both the maximally entangled and Bohm-Aharonov mixed states, depends on the azimuthal angle, which corresponds to the orientation of the scattering plane of the signal photon. This Stokes vector subtends an angle of 2ϕ relative to the *negative* S'_{01} -axis.

Using Eq. (18), the degree of polarization for the idler and signal beams, both before and after scattering, can be expressed for the entangled and mixed states as

$$\begin{aligned} p_i(\rho_{\text{en}}) &= 0, & p_s(\rho_{\text{en}}) &= 0 \quad (\text{before}), \\ p'_i(\rho_{\text{en}}) &= p', & p'_s(\rho_{\text{en}}) &= p' \quad (\text{after}), \end{aligned} \quad (38a)$$

and

$$\begin{aligned} p_i(\rho_{\text{ls}}) &= 0, & p_s(\rho_{\text{ls}}) &= 0 \quad (\text{before}), \\ p'_i(\rho_{\text{ls}}) &= \frac{p'}{2}, & p'_s(\rho_{\text{ls}}) &= p' \quad (\text{after}). \end{aligned} \quad (38b)$$

The results of Eqs. (38a) and (38b) for the postscattering (after) case are plotted in Fig. 9. They demonstrate that when the annihilation photons are in the maximally entangled state ρ_{en} , the degree of polarization of the signal and idler beams remains identical before and after scattering, irrespective of the azimuthal or polar scattering angles. In contrast, in the Bohm-Aharonov mixed state ρ_{ls} —where entanglement is absent but cross-polarization correlations persist—the degree of polarization of the idler beam after scattering of the signal photon is always half that of the signal beam, irrespective of the azimuthal or scattering angle. Since the key distinction between the entangled state and the Bohm-Aharonov mixed state is the absence of entanglement of the initial state in the latter, this result suggests that entanglement of the initial state preserves the polarization symmetry between the idler and signal beams after Compton scattering. Furthermore, the preserved symmetry in the degree of polarization between the signal and idler beams constitutes a measurable property of the system and can be regarded as a defining characteristic of the final two-photon state as a whole.

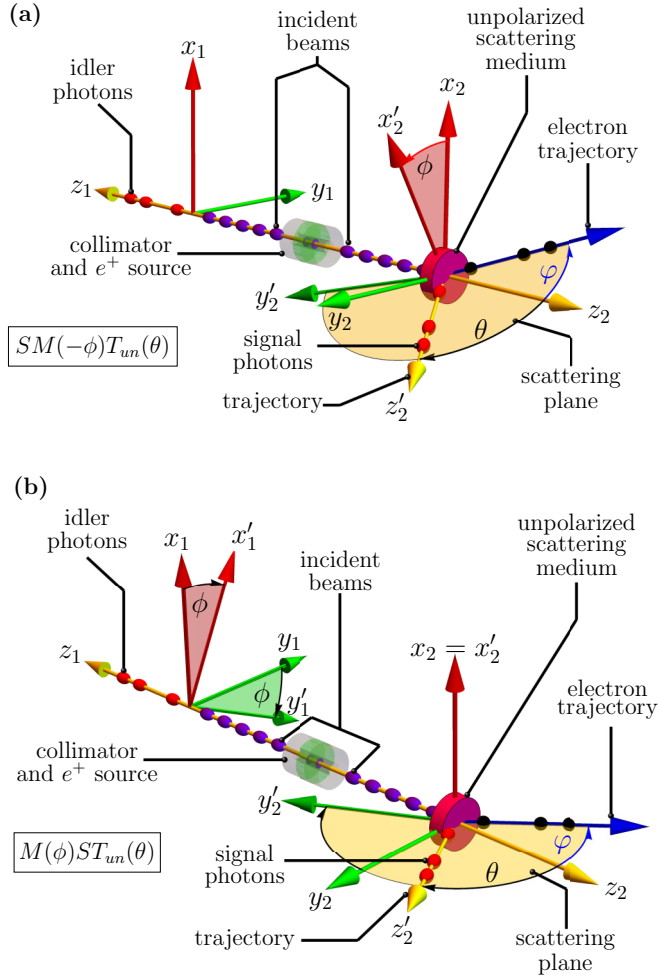


FIG. 7. (a) Rotation of the coordinate system of subsystem 2 about the z_2 -axis by an angle ϕ , while the coordinate system of subsystem 1 remains fixed; (b) the reverse configuration, where the coordinate system of subsystem 1 rotates while subsystem 2 remains fixed. Both geometries are equivalent [Eq. (34)], yielding the same evolved Stokes density matrix S' representing either state ρ_{en} or ρ_{ls} .

It is important to emphasize that the apparent change in the Stokes vector of the idler photon following Compton scattering of the signal photon, given in Eq. (37), does not imply a violation of locality or the no-signaling theorem. In this formalism, the evolved Stokes vector of the idler represents a conditional polarization state, reconstructed under the assumption that the signal photon has scattered into a known (θ, ϕ) direction and has been detected in coincidence with the idler. This corresponds to a postselected subensemble and is fully consistent with the framework of quantum steering. However, when the signal photon is not postselected—that is, when no information about its scattering direction is retained—the true reduced state of the idler, obtained by tracing over the signal subsystem, remains unchanged.

This result can be confirmed by integrating over the scattering and azimuthal angle in the expressions for the Stokes vectors $|\hat{S}'_i(\rho_{\text{en}})\rangle$ and $|\hat{S}'_i(\rho_{\text{ls}})\rangle$, given in Eqs. (37a) and (37b), respectively. This integration eliminates the conditional dependence on the scattering geometry of the signal

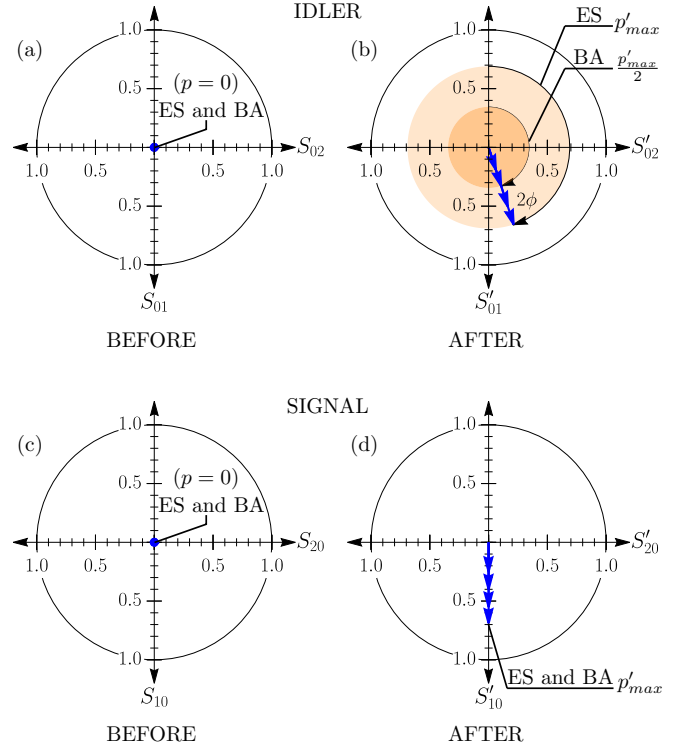


FIG. 8. The Stokes vector space on the equatorial plane of the Poincaré sphere, defined by the S_1 and S_2 axes, for the idler and signal beams before and after Compton scattering. Plots (a) and (c) show the Stokes vectors for the idler and signal beams in the entangled state (ES) and Bohm Aharonov (BA) mixed states prior to interaction, respectively. Plots (b) and (d) depicts the space of state of the Stokes vector for the idler and signal beams, respectively, after scattering. In plot (b), the light orange region represents the possible positions of the idler Stokes vector in the case of the entangled state, with a magnitude ranging from 0 to p_{max} . The darker orange region indicates the state space of the mixed state, constrained between 0 and $p_{\text{max}}/2$. Plot (d) shows that the Stokes vector for the signal beam is the same in both cases, confined along the positive S'_{10} axis, with a magnitude between $0 \leq p' \leq p'_{\text{max}}$, where $p'_{\text{max}} = 0.69$.

and recovers the original unpolarized state associated with the idler. For the entangled case, define $|\hat{S}'_i(\rho_{\text{en}})\rangle_{\text{av}}$ as the θ - and ϕ -averaged Stokes vector such that

$$|\hat{S}'_i(\rho_{\text{en}})\rangle_{\text{av}} = \frac{1}{4\pi} \int_{\theta=0}^{\pi} \int_{\phi=0}^{2\pi} |\hat{S}'_i(\rho_{\text{en}})\rangle d\Omega = \begin{bmatrix} 1 \\ 0 \\ 0 \\ 0 \end{bmatrix}, \quad (39a)$$

and similarly for the Bohm-Aharonov mixed case,

$$|\hat{S}'_i(\rho_{\text{ls}})\rangle_{\text{av}} = \frac{1}{4\pi} \int_{\theta=0}^{\pi} \int_{\phi=0}^{2\pi} |\hat{S}'_i(\rho_{\text{ls}})\rangle d\Omega = \begin{bmatrix} 1 \\ 0 \\ 0 \\ 0 \end{bmatrix}, \quad (39b)$$

where $d\Omega = \sin\theta d\phi d\theta$.

Equations (39a) and (39b) demonstrate that, in both cases, the reduced state of the idler remains maximally mixed after tracing over the signal. That is, when measurement outcomes associated with the signal photon are averaged out, the Stokes

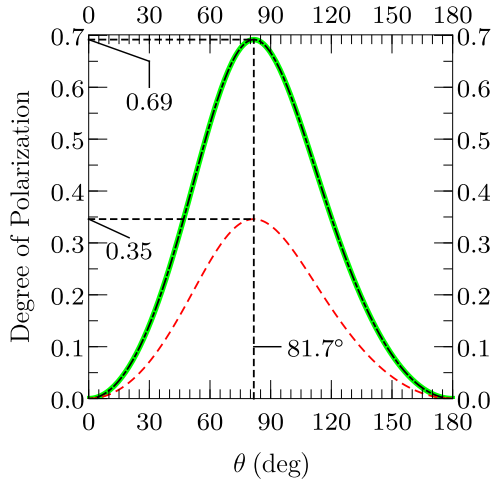


FIG. 9. Degree of polarization as a function of the Compton scattering angle θ for 511 keV photons. The green curve (—) corresponds to the single beam analysis presented in Fig. 3 and is plotted here for reference. The (---) curve represents $p'_s(\rho_{is})$, the degree of polarization of the signal beam in the Bohm-Aharonov mixed state, as well as $p'_i(\rho_{en})$ and $p'_s(\rho_{en})$, the degrees of polarization of the idler and signal beams when the photons are in a maximally entangled state. The (- - -) curve shows $p'_i(\rho_{is})$, the degree of polarization of the idler beam in the Bohm-Aharonov mixed state, which is consistently half that of the signal beam across all scattering angles.

vector of the idler remains unchanged, regardless of whether or not the signal has scattered. As a result, the reduced density matrix of the idler remains invariant under the partial trace operation.

It is useful to compute the joint differential cross-section for both the maximally entangled and Bohm-Aharonov mixed states in the setup shown in Fig. 7. Using the formula in Eq. (19), the joint differential cross-section for the evolved Stokes density matrices—corresponding to the entangled state in Eq. (35a) and the Bohm-Aharonov mixed state in Eq. (35b)—is given by

$$\frac{1}{4} \langle I_1 | S'(\rho_{is}) | I_2 \rangle = \frac{1}{4} \langle I_1 | S'(\rho_{en}) | I_2 \rangle = \frac{1}{4} \frac{d\sigma}{d\Omega}, \quad (40)$$

where $d\sigma/d\Omega$ is the differential scattering cross-section obtained from the single-photon beam analysis in Sec. III, Eq. (13). Equation (40) with Eq. (13) are plotted in Fig. 10.

VI. CONCLUSION

A key finding of this work lies in the polarization symmetry between subsystems of the annihilation photons in the maximally entangled state. The degree of polarization of the idler beam is identical to that of the signal beam across all scattering angles (θ, ϕ). In contrast, the Bohm-Aharonov mixed state—lacking entanglement—exhibits a broken symmetry, with the idler beam showing only half the degree of polarization of the signal beam. This contrast suggests that entanglement may play a role in preserving subsystem symmetry and points to a potentially accessible observable for distinguishing entangled from classically correlated photon states in specific scattering scenarios.

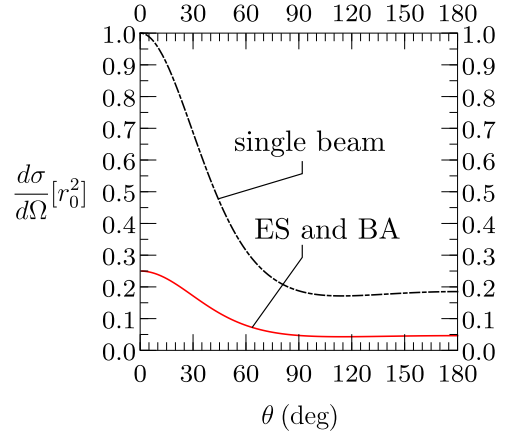


FIG. 10. Differential cross section (in units of r_0^2) for a single unpolarized 511 keV photon beam (---), and for a two-photon system in the maximally entangled state (ES) and the Bohm-Aharonov (BA) mixed state (—). As shown, the differential cross section is identical in both two-photon cases, indicating that coincidence measurements alone cannot distinguish between entangled and classically correlated photon pairs.

It is emphasized that the apparent change in the Stokes vector of the idler photon following Compton scattering of the signal photon does not imply a violation of locality or the no-signaling theorem. In this formalism, the Stokes vector of the idler represents a conditional polarization state—one reconstructed under the assumption that the signal photon scattered into a known direction and was subsequently detected in coincidence. This conditionality defines a postselected subensemble, fully consistent with quantum mechanics.

A plausible experimental strategy for accessing this conditional state would involve allowing the idler photon to undergo Compton scattering, with its angular distribution recorded on a position-sensitive detector placed downstream. Although the beam would also contain photons whose partners did not scatter, coincidence timing can, in principle, be used to isolate the relevant signal-idler pairs. This would leave primarily the scattering pattern of the idler, from which its Stokes vector can be inferred. The signal photon, by contrast, could be measured using a standard photon counter, provided its azimuthal and polar scattering angles are known. This kind of setup illustrates how quantum steering effects could be observed without invoking nonlocal signaling.

When all scattering directions of the signal photon are integrated over—that is, when no information about its outcome is retained—the reduced density matrix of the idler reverts to its original, unpolarized form. This invariance underscores a central conceptual result: although the two-photon state remains nonlocal in the quantum sense, the Compton interaction itself is strictly local. It acts only on the signal photon and induces no change in the marginal state of the idler unless conditioned on a specific signal outcome. This behavior is consistent with relativistic causality and the no-signaling theorem, and it reinforces the distinction between entanglement-driven correlations and dynamical nonlocality.

This result aligns with the findings of Shivashankara [29], who used a framework based on quantum field theory and

QED scattering amplitudes to model the interaction between an unpolarized electron and a photon from a Bell pair—specifically, the same entangled state commonly used to describe annihilation photons.

While the present work is theoretical in scope, the closed-form expressions derived for multiple Compton scattering—particularly in the context of entangled annihilation photons—offer an accessible framework for practical implementation. The ability to evaluate joint differential cross sections in compact analytic form enables a more straightforward integration into simulation platforms such as GEANT4, making the formalism suitable for research and development projects.

This opens the door to systematic studies of how entanglement affects the polarization correlations of annihilation photons undergoing multiple scattering events in PET detectors. In particular, the framework facilitates modeling of emerging Compton-PET architectures, where entanglement-sensitive corrections to scattering distributions may influence image reconstruction and detector response. While direct experimental validation of higher-order scattering effects (e.g., beyond 3-Compton) would likely require intense positron-emitting sources and high-statistics datasets, the immediate opportunity lies in using this theory to quantify systematic effects due to multiple scattering within detector media [22]. Embedding this model in Monte Carlo simulations could help isolate subtle entanglement-induced features, guide detector design, and strengthen the interpretability of experimental data without necessitating large-scale dedicated experiments in the near term.

Looking ahead, the formalism developed here establishes a platform for further theoretical exploration of entanglement dynamics in high-energy scattering regimes. In particular, the ability to spectrally decompose postscattering states and compute entanglement measures such as quantum concurrence provides a route to quantifying residual correlations after partial decoherence. These tools may prove valuable not only for foundational studies of entanglement under Lorentz-invariant interactions, but also for guiding detector design and data analysis in advanced PET and Compton imaging systems. Future work will focus on refining these tools and applying them to increasingly realistic geometries and scattering configurations.

ACKNOWLEDGMENTS

This work was partially supported by the Science and Technology Facilities Council (STFC) Grant No. ST/W006383/1.

DATA AVAILABILITY

The data that support the findings of this article are not publicly available upon publication because it is not technically feasible and/or the cost of preparing, depositing, and hosting the data would be prohibitive within the terms of this research project. The data are available from the authors upon reasonable request.

-
- [1] C. A. Kierans, S. E. Boggs, A. Zoglauer, A. W. Lowell, C. Sleator, J. Beechert, T. J. Brandt, P. Jean, H. Lazar, J. Roberts, T. Siegert, J. A. Tomsick, and P. von Ballmoos, Detection of the 511 keV galactic positron annihilation line with COSI, *Astrophys. J.* **895**, 44 (2020).
 - [2] H. Yoneda, H. Odaka, Y. Ichinohe, S. Takashima, T. Aramaki, K. Aoyama, J. Asaadi, L. Fabris, Y. Inoue, G. Karagiorgi, D. Khangulyan, M. Kimura, J. Leyva, R. Mukherjee, T. Nakasone, K. Perez, M. Sakurai, W. Seligman, M. Tanaka, N. Tsuji, K. Yorita, and J. Zeng, Reconstruction of multiple Compton scattering events in MeV gamma-ray Compton telescopes towards GRAMS: The physics-based probabilistic model, *Astropart. Phys.* **144**, 102765 (2023).
 - [3] C. Keith and D. Hooper, 511 keV excess and primordial black holes, *Phys. Rev. D* **104**, 063033 (2021).
 - [4] V. I. Grafutin and E. P. Prokop'ev, Positron annihilation spectroscopy in materials structure studies, *Phys. Usp.* **45**, 59 (2002).
 - [5] V. D. Irby, Physical limitations on quantum nonlocality in the detection of photons emitted from positron-electron annihilation, *Phys. Rev. A* **67**, 034102 (2003).
 - [6] I. Gauthier and M. Hawton, Photon correlations in positron annihilation, *Phys. Rev. A* **81**, 062121 (2010).
 - [7] S. Watanabe, S.-n. Ishikawa, H. Aono, S. Takeda, H. Odaka, M. Kokubun, T. Takahashi, K. Nakazawa, H. Tajima, M. Onishi, and Y. Kuroda, High energy resolution hard X-ray and gamma-ray imagers using CdTe diode devices, *IEEE Trans. Nucl. Sci.* **56**, 777 (2009).
 - [8] M. Frandes, A. Zoglauer, V. Maxim, and R. Prost, A tracking Compton-scattering imaging system for hadron therapy monitoring, *IEEE Trans. Nucl. Sci.* **57**, 144 (2010).
 - [9] M. Uenomachi, M. Takahashi, K. Shimazoe, H. Takahashi, K. Kamada, T. Orita, K. Ogane, and A. B. Tsuji, Simultaneous in vivo imaging with PET and SPECT tracers using a Compton-PET hybrid camera, *Sci. Rep.* **11**, 17933 (2021).
 - [10] D. Abdurashitov, A. Baranov, D. Borisenko, F. Guber, A. Ivashkin, S. Morozov, S. Musin, A. Strizhak, I. Tkachev, V. Volkov, and B. Zhuikov, Setup of Compton polarimeters for measuring entangled annihilation photons, *J. Instrum.* **17**, P03010 (2022).
 - [11] P. Caradonna, D. Reutens, T. Takahashi, S. Takeda, and V. Vegh, Probing entanglement in Compton interactions, *J. Phys. Commun.* **3**, 105005 (2019).
 - [12] B. C. Hiesmayr and P. Moskal, Witnessing entanglement in Compton scattering processes via mutually unbiased bases, *Sci. Rep.* **9**, 8166 (2019).
 - [13] P. Caradonna, I. D'Amico, D. G. Jenkins, and D. P. Watts, Stokes-parameter representation for Compton scattering of entangled and classically correlated two-photon systems, *Phys. Rev. A* **109**, 033719 (2024).
 - [14] P. Caradonna, Kinematic analysis of multiple Compton scattering in quantum-entangled two-photon systems, *Ann. Phys.* **470**, 169779 (2024).
 - [15] A. L. McNamara, M. Toghyani, J. E. Gillam, K. Wu, and Z. Kuncic, Towards optimal imaging with PET: An *in silico* feasibility study, *Phys. Med. Biol.* **59**, 7587 (2014).

- [16] H. Eslami and M. Mohamadian, Optimization of the positron emission tomography image resolution by using quantum entanglement concept, *Eur. Phys. J. Plus* **139**, 976 (2024).
- [17] D. Kim, A. N. Rachman, U. Taisei, M. Uenomachi, K. Shimazoe, and H. Takahashi, Background reduction in PET by double Compton scattering of quantum entangled annihilation photons, *J. Instrum.* **18**, P07007 (2023).
- [18] G. R. Romanchek, S. Greyson, and A. Shiva, Application of quantum entanglement induced polarization for dual-positron and prompt gamma imaging, *Bio-Alg. Med-Syst.* **19**, 9 (2023).
- [19] A. M. Kožuljević, T. Bokulić, D. Grošev, Z. Kuncic, S. Parashari, L. Pavelić, and M. Makek, Investigation of the spatial resolution of PET imaging system measuring polarization-correlated Compton events, *Nucl. Instrum. Methods Phys. Res., Sect. A* **1068**, 169795 (2024).
- [20] M. H. L. Pryce and J. C. Ward, Angular correlation effects with annihilation radiation, *Nature (London)* **160**, 435 (1947).
- [21] H. S. Snyder, S. Pasternack, and J. Hornbostel, Angular correlation of scattered annihilation radiation, *Phys. Rev.* **73**, 440 (1948).
- [22] J. Bordes, J. R. Brown, D. P. Watts, M. Bashkanov, K. Gibson, R. Newton, and N. Zachariou, First detailed study of the quantum decoherence of entangled gamma photons, *Phys. Rev. Lett.* **133**, 132502 (2024).
- [23] I. Tkachev, S. Musin, D. Abdurashitov, A. Baranov, F. Guber, A. Ivashkin, and A. Strizhak, Measuring the evolution of entanglement in Compton scattering, *Sci. Rep.* **15**, 6064 (2025).
- [24] A. Wightman, Note on polarization effects in Compton scattering, *Phys. Rev.* **74**, 1813 (1948).
- [25] W. H. McMaster, Matrix representation of polarization, *Rev. Mod. Phys.* **33**, 8 (1961).
- [26] A. F. Abouraddy, A. V. Sergienko, B. E. Saleh, and M. C. Teich, Quantum entanglement and the two-photon Stokes parameters, *Opt. Commun.* **201**, 93 (2002).
- [27] D. Bohm and Y. Aharonov, Discussion of experimental proof for the paradox of Einstein, Rosen, and Podolsky, *Phys. Rev.* **108**, 1070 (1957).
- [28] D. J. Bohm and B. J. Hiley, Nonlocality and polarization correlations of annihilation quanta, *Nuovo Cim B* **35**, 137 (1976).
- [29] S. Shivashankara, Entanglement entropy of Compton scattering with a witness, *Can. J. Phys.* **101**, 757 (2023).